# Novel thermomechanical characterization for shrinkage evolution of unidirectional semi-crystalline thermoplastic prepregs (PPS/CF) in melt, rubbery and glassy states

Golzar, M.; Sinke, J.; Abouhamzeh, M.

**DOI**
10.1016/j.compositesa.2022.106879

**Publication date**
2022

**Document Version**
Final published version

**Published in**
Composites Part A: Applied Science and Manufacturing

Composites: Part A 156 (2022) 106879

Contents lists available at ScienceDirect

Composites Part A

journal homepage: www.elsevier.com/locate/compositesa

# Novel thermomechanical characterization for shrinkage evolution of unidirectional semi-crystalline thermoplastic prepregs (PPS/CF) in melt, rubbery and glassy states

M. Golzar [a,*], J. Sinke [b], M. Abouhamzeh [c]

[a] Faculty of Mechanical Engineering, Tarbiat Modares University, P.O. Box 14115-143, Tehran, Iran
[b] Department of Aerospace Structures & Materials, AE, Technical University of Delft, Kluyverweg1, 2619HS Delft, Netherlands
[c] Institute of Aircraft Design and Lightweight Structures, Technische Universität Braunschweig, Hermann-Blenk-Str. 35, 38108 Braunschweig, Germany

ARTICLE INFO

*Keywords:*
A. Prepreg
A. Thermoplastic resin
B. Thermomechanical
D. Physical methods of analysis

ABSTRACT

Shrinkages, distortions and high residual stresses in the thermoplastic composite parts are induced due to high processing temperature, anisotropy, and fiber–matrix shrinkage mismatch. In this paper the shrinkages have been investigated experimentally and modeled by thermo-mechanical constitutive equations for PolyPhenylene Sulfide (PPS) and the unidirectional Carbon Fiber (PPS/CF) composite prepreg. The thermal shrinkage and the crystallization shrinkage were retrieved from Thermal Mechanical Analysis and compared to a Pressure specific volume Temperature diagram. To describe the crystallization shrinkage in the cooling process accurately, the crystallization kinetics of PPS was evaluated using Differential Scanning Calorimetry. The temperature-dependent elastic modulus was measured by a shear rheometer to formulate a new constitutive model. The mathematical model for shrinkage was validated by a press consolidated $[0]_{12}$ laminate and unbalanced laminates in four lay-ups. The thermo-mechanical model results presented here provide significant rules for the thermomechanical and shrinkage predictions for the industrial applications of thermoplastic composite.

## 1. Introduction

Unidirectional fiber reinforced thermoplastic composites offer excellent lightweight products for aerospace, automotive and have potential applications in wind turbine structures. In addition to recycling, thermoplastic composites provide advantages over the thermoset ones like lower processing time, higher toughness, ductility, good chemical resistance, formability and weld-ability. However, there are still some challenges due to their high viscosity, higher cost and higher temperatures in the production process. Because high-performance thermoplastic composites are produced by processing temperature above 300 °C, cooling shrinkage rises up because of crystallinity, which is increased by increasing process temperature and cooling rate.

Although high-performance thermoplastic composites have been widely utilized for over 40 years and their properties are well defined, accurate models to predict the shrinkage need to be developed and improved using modern equipment. In-depth studies have been published on thermoplastic composite distortions and residual stresses about the experimental and theoretical studies on thermoplastic matrix [1,2]. Although, the simulation tools are well developed in thermoset composite and hybrid structures [3,4,5], more research on thermoplastic behavior need to be performed. As the demand for thermoplastic matrix composites is increasing, accurate modeling to understand shrinkage behavioral is needed, therefore in this paper research is performed on thermo-mechanical properties of industrial thermoplastic prepregs to use in PPS/CF composites. Because thermoplastic production requires much higher temperatures than the thermoset matrix, a wide range of temperature and cooling rate properties are analyzed. Instead of the irreversible curing process in thermoset composites, thermoplastic solidification is a reversible procedure: so, it must be heated up to the process temperature to soften and cooled down to solidify the final product. Another distinction for thermosets is the degree of curing, which is time and temperature dependent, while for semi-crystalline thermoplastics the degree of crystallinity depends on crystallization kinetics, like temperature, cooling rate and environmental effects.

The shrinkage of the thermoplastic composites consists of two types, occurring during cooling from process to room temperature. The first

* Corresponding author.
*E-mail address:* m.golzar@modares.ac.ir (M. Golzar).

https://doi.org/10.1016/j.compositesa.2022.106879
Received 18 October 2021; Received in revised form 6 February 2022; Accepted 7 February 2022
Available online 22 February 2022

shrinkage type, the thermal one, is described by the Coefficient of Thermal Expansion (CTE). The thermal contraction occurs due to losing of the thermal energy of macro-molecules by solidification in cooling process. The thermal expansion happens during the heating which is repeatable after the contraction during cooling. The second type is the Crystallization Shrinkage (CS), which reflects the volume decrease by exothermic transformation from melt to rubbery state by crystallization and is quantitated by the Degree Of Crystallization (DOC). The crystallization shrinkage takes place in a reversible physical process for thermoplastics. Therefore, the thermal shrinkage is common in both thermoplastic and thermoset composites which is the first type of shrinkage (CTE), but the second types of shrinkage have different source, thermosets have curing shrinkage which is irreversible process while thermoplastics crystallize with physical reversible phenomena.

Chapman et al. [6] focused on the residual stresses of thermoplastic composites and discussed shrinkage of PEEK (PolyEtherEtherketone). They showed how the coefficient of thermal expansion (CTE) changes during cooling. Although constant contraction is normally considered below $T_g$ and above the crystallization temperature, they noticed an additional expansion due to the second crystallization. They concluded that the difference between thermal shrinkage and crystallization seems difficult tomeasure. Lawrence et al. [7] divided the thermoplastic shrinkage contributions into heat and crystallization and determined the unidirectional fiber composite shrinkage by micromechanics. For neat PEEK and CF / PEEK composites, they concluded that crystallization and cooling rate had small effect on the overall shrinkage and the final value of the process-induced strains, however the CTE played a dominant role. They observed that the PEEK elastic modulus versus temperature change is a possible cause of stress and distortion at different crystallization values. Barnes et al. [8] investigated directly the CTE of thermoplastic composites by laser interferometer equipment and found that shrinkages over temperature have U-shaped variation, they confirmed that shrinkages for different angle plies are related to principal ply direction. For Glass Mat Thermoplastic and other thermoplastic composites, Trende et al investigated the compression molding residual stresses, by calculating volume change and superimposing the thermal shrinkage to the crystallization shrinkage to find the total shrinkage [9]. Based on dimensional variations of thermoplastic composites using viscoelasticity Kim et al. [10] extracted the shrinkage of PA12. They assumed an isotropic incremental volumetric shrinkage, relying on the density dependent crystallinity [7]. Besides, they inserted density by crystallinity content, amorphous density and full crystalline densities in rule of mixture. Brauner et al. [11] computed the composite CTE by micromechanics and discovered less shrinkage in the longitudinal direction, while in the transverse direction the shrinkage had no crystallinity dependency; therefore, they concluded that the transverse shrinkage is primarily induced by matrix contraction. Recently, Greisel et al. [12] introduced the representative CTE versus temperature for the PPS/CF in three different heating cycles. They reported that the irreversible thermal expansion is due to the relaxation of the process-induced residual stress, because the moisture absorption of PPS is negligible and the thermal treatment did not influence the degree of crystallinity of the samples Normally the moisture absorption is different for polymers and leads to dimensional variations and mechanical degradation. Moisture changes the thermoplastic composite properties which has been recently investigated for PPS [13]. Furthermore, the moisture effect can be reduced during processing and by heat treatment [14].

Some researchers focused on modelling the manufacturing process of the thermoplastic composite parts [15,16]. Recently, the properties of commercial thermoplastics have been extensively characterized [3,17,18,19]. However, that accurate and comprehensive thermo-mechanical and viscoelastic properties are not presented in the existing studies. The identification of thermomechanical behaviour of thermoplastic composites in cooling from melt to room temperature are not sufficiently supported by both laboratory examination and manufacturing facilities. The present work offers a detailed model for the manufacturing of industrial thermoplastic composites PPS/CF prepregs. Accurate input will be provided in order to calculate the induced distortions. In this paper a new thermo-mechanical methodology is introduced for evolution characterization of thermoplastic composite prepregs. The techniques carried out on unidirectional PPS/CF, include (a) shear rheometer to investigate the elastic modulus during cooling, (b) TMA (Thermal Mechanical Analysis) to follow the strain variation evolving solid to rubber and viscous region with successive heating and cooling to identify the behavior during crystallization, (c) DSC (Differential Scanning Calorimetry) of neat thermoplastic and unidirectional prepregs of thermoplastic composite to investigate the crystallization kinetics. All measurements are presented graphically and are mathematically fitted by novel regression equations. The above-mentioned laboratory measurements and extracted evolution thermomechanical value are compared by data of press forming (d) Consolidated unidirectional laminates and (e) out of plane deformations in different unsymmetrical laminates. Finally, a micromechanical based CLT (Classical Lamination Theory) model is compared with the experimental results to validate the methodology.

Many studies have been performed on the measurement of thermal and transformation strains during processing of thermoset composites, but less are found in the case of thermoplastic composites, especially during crystallization.

## 2. Materials and methods

### 2.1. Materials

The semi-crystalline thermoplastic composite assayed in this manuscript is unidirectional carbon fiber and PolyPhenylene Sulphide (PPS) matrix. The unidirectional PPS/CF plies were on a roll of 315 mm width and 0.16 mm thickness from Phoenix TPC. The PPS neat semi-crystalline thermoplastic material is provided by TenCate Cetex TC1100 as transparent glassy films with 0.05 mm thickness.

### 2.2. Sample preparation

The heating and cooling cycle to produce PPS/CF flat laminates in compression molding is presented in Fig. 1 as well as the pressure over time. The temperature is raised to melt the thermoplastic, and then the pressure is increased to consolidate the laminate while the press is cooled down. The samples are heated under closed press, from room temperature by 7.5 °C/min up to 330 °C, hold the 330 °C temperature for 20 min, and the last step was the cooling by 15 °C/min. Flat UD laminates and strips are produced for the investigation. The UD plies are cut and the laminates with $[0]_{12}$ lay-up are made. The PPS/CF prepreg plies, from Phoenix TPC are first cut precisely using hand board cutter machine in 0 and 90° and laid up accurately in the layers and orientations and fixed by portable ultrasonic point welding machine. Thereafter the non-consolidated laminate is placed in Kapton foil envelop (2Mill 50 μ m) to prevent squeeze out of the unidirectional fiber and matrix at melt temperature. They are then consolidated between hot plates Joos press, which is located at the Delft Aerospace Structure and Materials Laboratory (DASML [20]. The shrinkage of the Kapton foil according to the producer is 1.25 % at 400 °C [21]. The press temperature was controlled by hot water and air. The temperature and pressure applied to the laminate are measured and shown in Fig. 1.

The bi-laminar strips from PPS/CF prepregs are arranged in an unsymmetrical lay up such that 4 plies are always in the longitudinal direction at the one side and 4 plies in the transverse direction on the other side of laminate. The manufacturing procedure of the bi-laminar specimens is applied in the same way as for the UD laminate.

The prepregs and the consolidated laminates are examined for density by method of water immersing according to ASTM D 792 and ISO 1183–1. If the weight of test specimen in air is $m$ and the weight of immersed in a water is $m_i$ the density can be calculated as $\rho = m/(m - m$

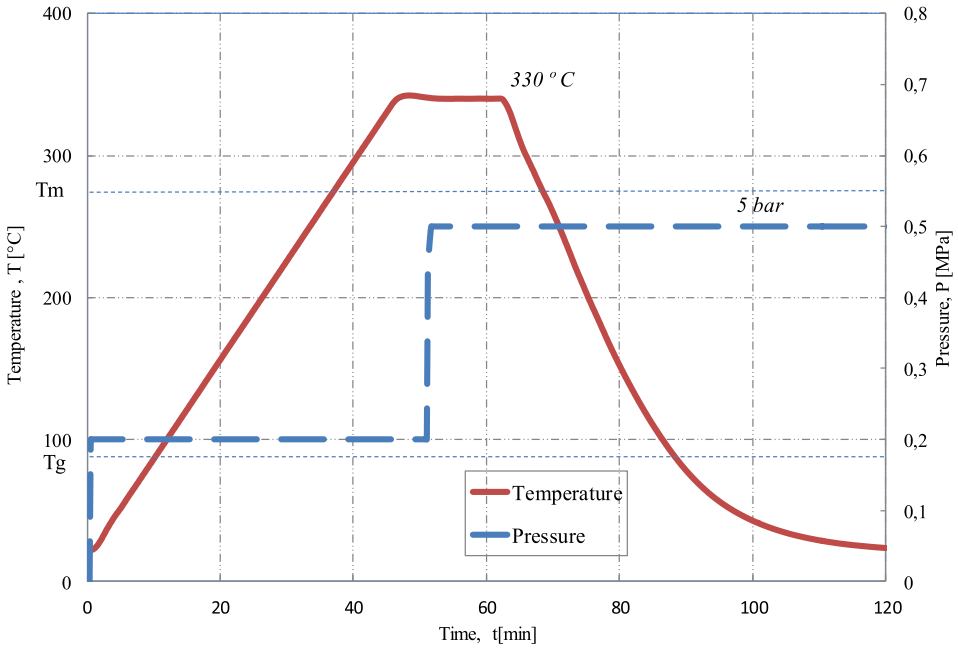


**Fig. 1.** Temperature and pressure in compression molding for PPS/CF consolidation laminate.

$_i$) in (gr/cm$^3$).

In Table 1, the densities of prepreg tape and each fabricated laminate are determined and compared. The density value of prepreg was lower than for the consolidated laminate, due to the process conditions, and void content. However, for consolidated unsymmetrical laminates the density values were calculated by dividing the laminates total weight by total volume, which leads to a good approximation. The density by rule of mixture is about 1.57 (gr/cm$^3$) for $V_f = 0.49$. The prepreg fiber volume content was determined using microscopy of epoxy mounted specimens. The PPS/CF void content was found near 1%±0.1% for prepreg, however the consolidated laminates $[0]_{12}$ have less than 1% ±0.1% void content.

The dimensions and the thickness of the PPS/CF laminates were measured by a micrometer at six points, and the average values are shown in the Table 2. The thickness variations were recorded to be about 0.8%, because the investigated specimen area (length × width) is smaller compared to the pressed laminate area (600mmX600mm). The pressed PPS/CF laminates show enlargement in width and length of 2% with respect to the original prepreg lamina.

The unsymmetrical lay-ups are selected and illustrated in Table 2 with different lamina sequences. In Table 2 the stacking sequences of unsymmetrical lay-ups are designed to have different strain evolutions during cooling, as the different curvatures are due to the internal thermal residual stress by consolidation. The unsymmetrically bi-laminates Table 2, decrease from a high to low degree of non-symmetry. The shrinkage in fiber direction is negligible because of high stiffness and small CTE. In the transverse direction (90°), the matrix is dominant and the stiffness increases by cooling and solidification from soft state to rubbery or glassy. The strip curvatures of consolidated laminates are measured by two methods. First by curvature measuring method, the maximum deflection and the total cord were measured and substituted in $\kappa = \frac{8h}{C^2+4h^2}$. The curvature $\kappa$ is given by trigonometry of the arc, where $h$ is the deflection and $c$ is the cord length and $\kappa$ is the curvature (the inverse of radius). While the second method is carried out by Digital Image Correlation (DIC) very similar to recent use by M. Peron et. Al. [22].

**Table 1**
Density of PPS/CF prepreg and consolidated laminates.

| | Density (gr/cm$^3$) | sample dimensions (mm × mm × mm) |
|---|---|---|
| prepregs tape (Phoenixx TPC) | 1.48 ± 2% | 20 × 15 × 0.12 |
| $[0]_{12}$ Laminates (consolidated as Fig. 1) | 1.57 ± 1% | 12 × 12 × 1.7 |
| $[0_4/90_4]$ Laminate (consolidated as Fig. 1) | 1.58 ± 1% | 300 × 50 × 1.1 |
| Rule of mixture ($V_f = 0.49$) | 1.57 | – |

### 2.3. Experimental equipment and methods

A shear rheometer makes it possible to measure the thermoplastic stiffness by a plate-to-plate small angle oscillation test for a neat PPS. The shear rheology is performed on a ThermoFischer Haake Mars III – Nicolet iS10 FT-IR [23]. The neat PPS foil of 0.5 mm thickness are cut in 30 mm width and 150 mm length. The 40 layers were stacked in aluminum mold, heated to 330 in vacuum oven and cooled down in 10 °C/min to room temperature. This neat PPS sample is punched in a circular disc with 8 mm diameter and 1.5 mm thickness, then it is placed between the rheometer plates, and heated to the temperature (~350 °C). The PPS angular deformation is recorded in response to the applied torque by the machine during the cooling down by −9°C/min to room temperature. The elastic shear modulus is extracted from the shear rheometer and is shown as a function of cooling time in Fig. 2 from the melt to the solid state.

Thermal Mechanical Analysis (TMA) is an accurate method for measuring the Coefficient of Linear Thermal Expansion (CLTE), but TMA is commonly used for solid and not for melt state polymers at different temperatures. The purpose of this paper is to identify the thermal shrinkage and crystallization shrinkage, so two experiments were designed to investigate PPS/CF by Perkin Elmer Diamond TMA equipment: the first in solid state and the second in the transition from the melt to the solid states.

### 2.4. TMA for solid state PPS/CF

To determine the CTE of the PPS/CF, the $[0]_{12}$ laminates are fabricated by compression molding thereafter cut in square samples with approximately 6mmX6mmX1.7 mm dimensions, and then placed under the probe of the TMA equipment. The samples are heated at a rate of 10 °C/min to the heat deflection temperature(~260 °C) [36] and cooled

**Table 2**
Dimensions and thickness variations of PPS/CF laminates.

| | $t_1$ | $t_2$ | $t_3$ | $t_{ave}$ | $l$ | $w$ |
|---|---|---|---|---|---|---|
| $[0]_{12}$ | 1.58 ± 0.3% | 1.61 ± 0.2% | 1.74 ± 0.2% | 1.6 ± 0.8% | 204 | 103 |
| $[0_4/90_4]$ | 1.05 ± 0.4% | 1.15 ± 0.3% | 1.27 ± 0.2% | 1.15 ± 0.8 % | 303 | 52 |
| Unsymetrical laminates of PPS/CF | | | | | | |
| $[0_4/90_4]$ | | $[0_3/90/0/90_3]$ | $[0_2/90_2]_2$ | | $[0/90]_4$ | |

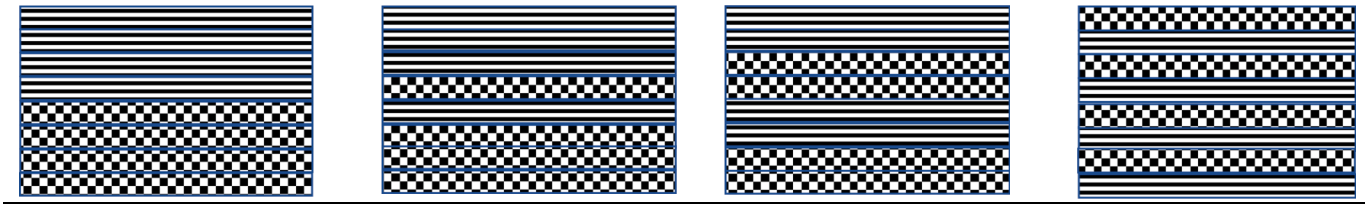

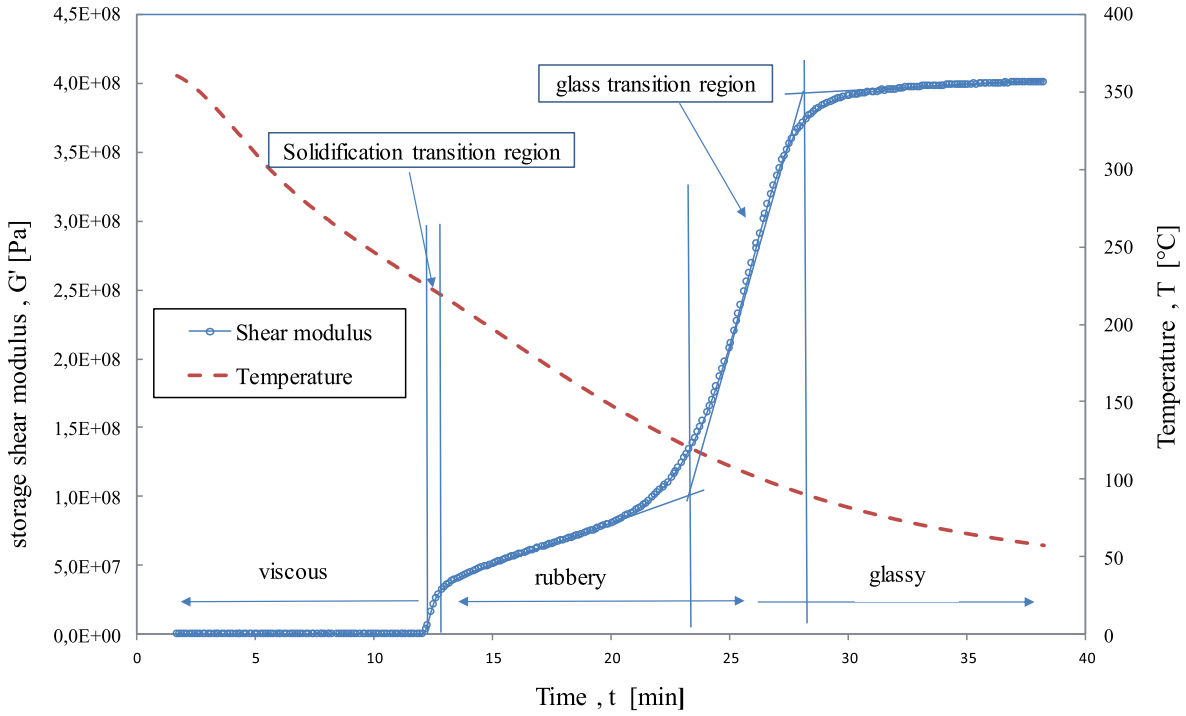


**Fig. 2.** Shear elastic modulus G' and temperature over time for semi-crystalline neat PPS.

with a rate of 10 °C/min twice sequentially. The heat deflection temperature is chosen to avoid probe penetration in the samples due to PPS softening at high temperature. The TMA probe measures the thickness variations like expansions and contractions.

The strain is first calculated from the thickness changes and then the $\alpha_{22}$ should be estimated by $\alpha_{22} = \frac{\varepsilon}{\Delta T} = (l - l_0)/l_0/(T - T_0)$. The calculations are a kind of differentiation, so it leads to a lot of strain fluctuations due to discontinuous thickness values recorded by the TMA equipment. The proposed way here is to fit a linear regression curve for the length versus temperature to find the relation $L(T) = \alpha_{22}(T).(T - T_0) + L$, so that the CLTE can be obtained from the linear expansion as $\alpha_{22} = \frac{1}{L}\frac{dL}{dT}$.

### 2.5. TMA for solid to molten PPS/CF

As mentioned earlier, the TMA equipment is not designed for measuring the CTE in the melting and softening region of thermoplastics prepregs. The first test in Fig. 4 was carried out from room temperature to the softening temperature (220 °C for PPS which is far below the melt temperature). In order to reach the melting point and capture the expansion in a viscous state, a consolidated $[0]_{12}$ PPS/CF sample in cylindrical shape was located in an aluminum pan (5 mm in diameter) and was covered with an aluminum head. The probe sensor (3 mm in diameter) was precisely placed on the cover with a slight compression force (5 m N) to maintain contact of the cover with the sample. When the aluminum pan is heated up and cooled down in an isolated chamber of the TMA equipment, the cover moves up and down by the PPS/CF samples expansion and contraction, while the sensor records the height of sample, and indicate the effect of CTE. To ensure the contact of the cover to the sample in contraction and softening states, the probe sensor force was increased (5 mN to 50 mN in 2 mN/min); see Fig. 5(a). The measurement was calibrated by an empty aluminum pan-cover, and the heating cycles were repeated with PPS/CF samples in order to find the suitable heating rate, cooling rate and probe force over time.

### 2.6. Dsc

The crystallization should be studied in the laboratory over time by the experimental method named the Differential Scanning Calorimetry (DSC). In this study DSC measurements were performed using Perkin Elmer DSC 8000 equipment. It needs 10 mg of thermoplastic in a pan to study the thermal behavior during heating and cooling.

To study the crystallization properly, the heating up to the process

temperature and cooling down to the room temperature can be repeated many times by the DSC equipment. The total time above melting temperature of the part under press according Fig. 1 is about 35 min. This time is adjusted to prevent degradation of the samples during the TMA and DSC successive heating/cooling cycles.

## 3. Theory of constitutive equation in cooling

Most of constitutive models are derived from thermo-mechanical and viscoelastic behavior of the material during shrinkage [10,24,25]. The total shrinkage is expressed by the composite strain during the cooling in Eq. (1), as an incremental summation of elastic strain, thermal strain, crystallization strain, strain due to moisture and viscous strain.

$$d\varepsilon_{ij}^{total} = d\varepsilon_{ij}^{elastic} + d\varepsilon_{ij}^{thermal} + d\varepsilon_{ij}^{crystallisation} + d\varepsilon_{ij}^{moisture} + d\varepsilon_{ij}^{viscos} \quad (1)$$

Where the suffix $i$ and $j$ are the tensor notation and are defined for three dimensions. The stress induced by the strains is derived from the Hooke's law for incremental elasticity and is described by Eq. (2).

$$d\sigma_{ij} = C_{ijkl}.d\varepsilon_{ij}^{elastic} \quad (2)$$

Where the $C_{ijkl}$ is the mechanical stiffness tensor. The linear stress–strain model from incremental linear elasticity describes well enough the shrinkage of thermoplastic prepregs [11,26]. After substituting the incremental elastic strain from Eq. (1) in Eq. (2) the constitutive model would take the form as in Eq. (3).

$$d\sigma_{ij} = C_{ijkl}.\left(d\varepsilon_{ij}^{total} - d\varepsilon_{ij}^{thermal} - d\varepsilon_{ij}^{crystallisation} - d\varepsilon_{ij}^{moisture} - d\varepsilon_{ij}^{viscos}\right) \quad (3)$$

In this study, it is assumed that the thermal strain and the crystallization strain in Eq. (3) does not affect the moisture strain and the viscous strain, so the simplified form in Eq. (4) is obtained for stresses raised by shrinkage. The moisture and viscous strains are not investigated here and the study focuses on the thermal and crystallization shrinkages.

$$d\sigma_{ij} = C_{ijkl}.\left(d\varepsilon_{ij}^{total} - d\varepsilon_{ij}^{thermal} - d\varepsilon_{ij}^{crystallisation}\right) \quad (4)$$

The thermal strain and crystallization strain together can be measured directly or estimated by micromechanical formulation and could be named shrinkage because the thermoplastic prepreg normally shrink from the melt to the solid states during cooling. The thermal strain is estimated by the thermal shrinkage matrix $\alpha_{ij}$ and it is assumed to be proportional to the temperature difference; however, the crystallization strain is calculated by crystallization shrinkage matrix and is proportional to the degree of crystallization DOC. The thermal shrinkage is assumed to be temperature dependent, but not crystallization (DOC) dependent, as stated in Eq. (5).

$$d\sigma_{ij} = C_{ijkl}.\left(d\varepsilon_{ij}^{total} - \alpha_{ij}.dT - \alpha_{ij}.dX\right) \quad (5)$$

Where the $\alpha_{ij}$ is the thermal expansion or shrinkage tensor and the $\gamma_{ij}$ is the crystallization shrinkage tensor [27]. $X$ is the degree of crystallization (DOC) and gets a value from zero for an amorphous (non-crystalline) to one for a full crystalline polymer. For semi-crystalline polymers, the DOC varies between zero and one ($0 < X < 1$) and it depends on the thermoplastic macromolecules, the manufacturing process and the cooling procedure.

Using micromechanics is a well-known method for estimating the unidirectional composite CTE, residual stresses and shrinkages-warpages [10,24,28]. The Micromechanics formulations are based on the fiber volume fraction of the composites besides fiber and matrix shrinkages as well as elastic properties. The thermal and crystallization shrinkage in Eq. (5) are derived from micromechanics for PPS/CF unidirectional prepregs in the longitudinal and in the transverse directions in Eq. (6) [29]:

$$\alpha_{11} = \frac{\alpha_{1f}.E_{1f}.V_f + \alpha_m.E_m.(1-V_f)}{E_{1f}.V_f + E_m.(1-V_f)}$$
$$\alpha_{22} = \alpha_{33} = (\alpha_{2f} + \alpha_{1f}.\nu_{12f}).V_f + (1+\nu_m).\alpha_m.(1-V_f) - \nu_{12}.\alpha_1 \quad (6)$$

Where the index $f$ and $m$ indicate the fiber and matrix. Fibers' Poisson's ratios are considered constant, the thermoplastic Poisson's ratio from room to melt state increases, but have no significant effect on the composite shrinkages. In order to express the crystallization shrinkage of the unidirectional prepreg in a homogenized form, the micromechanical thermal shrinkages in Eq. (6) are assumed to be valid if the fiber crystallization shrinkage is zero. The formulas for longitudinal crystallization shrinkage and transverse crystallization shrinkage are given in Eq. (7):

$$\gamma_{11} = \frac{\gamma_m.E_m.(1-V_f)}{E_{1f}.V_f + E_m.(1-V_f)}$$
$$\gamma_{22} = \gamma_{33} = (1+\nu_m).\gamma_m.(1-V_f) - \nu_{12}.\gamma_1 \quad (7)$$

For the mentioned specific thermoplastic prepregs the thermal shrinkage and crystallization shrinkage are dependent on temperature and cooling rate. The material properties for carbon fiber and PPS, are listed in Table 3 for room temperature. The aim of this paper is to develop a model for the thermomechanical properties for higher temperatures.

Thermoplastics composites crystallize differently due to fiber reinforcement type, reinforcement architecture, manufacturing and post-processing conditions. The high performance semi-crystalline polymers like PPS have different crystals and DOC. Golzar [30] discussed the properties for a semi-crystalline polymer as a function of DOC, amorphous property and crystalline property. Consequently, it is rather difficult to determine the shrinkage of amorphous and crystalline parts separately, therefore the sum of thermal and crystallization shrinkages of thermoplastics are the objective of this paper. As the first step the elastic modulus $E_m$ is required as the function of temperature and crystallization to insert in Eq. (6) and Eq. (7).

## 4. Results and discussion

### 4.1. Elastic stiffness of thermoplastic matrix

The elastic modulus of a thermoplastic polymer changes significantly with temperature and has an important impact on shrinkage of matrix and composites. Measuring the thermoplastic elastic modulus is possible when temperatures are far below the melting temperature, i.e. for PPS or PPS/CF up to 220 °C. The matrix elastic modulus is utilized in the micromechanics formulas to homogenize the composite elastic properties [6,9,10,11,19,26]. The elastic shear modulus is extracted from the shear rheometer in Fig. 2 during cooling time from the melt to the solid state. For the PPS matrix, as an isotropic thermoplastic the relation in Eq. (8) is valid for the elastic modulus.

$$E = 2.G^{'}.(1+\nu_m) \quad (8)$$

In Eq (8), $E$ is the Young's modulus, $G^{'}$ is the elastic shear modulus and

**Table 3**
Carbon fiber and PPS properties at 25 °C.

| | $E_1$ (GPa) | $E_2$ (GPa) | $G_{12}$ (GPa) | $\nu_{12}$ | $\alpha_1$(1e-6/°C) | $\alpha_2$(1e-6/°C) | ρ (gr/cm$^{3)}$ |
|---|---|---|---|---|---|---|---|
| Carbon Fiber | 230 | 22 | 22 | 0.3 | −1.3 | 7 | 1.8 |
| Matrix PPS [37] | 3.8 | 3.8 | 1.4 | 0.36 | 52 | 52 | 1.34 |
| PPS/CF | 137.5 | 4.2 | 4.4 | 0.33 | −0.6 | 35 | 1.57 |

$\nu_m$ is the Poisson's ratio of PPS. Decreasing the temperature of the molten PPS, causes the macromolecules coming closer (Van der Waals bonding), therefore the melt elastic modulus increases slightly. By further cooling, the solidification starts, and the PPS elastic modulus increases rapidly by forming the crystalline parts; at lower temperatures whereas the PPS amorphous part is frozen at $T_g$, the PPS elastic modulus increases further. The experimental results from shear rheometer are extracted and presented in Fig. 2 for PPS elastic modulus versus temperature. The solid, rubbery and melt states of PPS are indicated in three thermoplastic regions. The starting point of solidification is assumed to be the start of stiffness raising during cooling, when the PPS macromolecules start to build up the crystal structure depending on the cooling rate and the external force. After the initial solidification the elastic stiffness tends to increase linearly by cooling and makes a second increase into the glassy region.

For the thermoplastic semi-crystalline elastic modulus, Eq. (9) is devoted ; which is recently suggested and applied for thermoset prepregs [19] elastic modulus as a function of temperature:

$$E_{rg}\left(T, T_c^{onset}\right) = \sum_{n=1}^{N} \frac{E_n}{1+\exp\left(\frac{(T-T_c^{onset})+\delta T_n}{\tau_n}\right)} \tag{9}$$

Where $E_{rg}$ is the elastic modulus in rubber-glassy state of the thermoplastic. The degree of crystallization enters the elastic model as $T_c^{onset}$, which depends on the cooling rate. By cooling down, the elastic modulus increases at $T_c^{onset}$ temperature; this temperature is the crystal formation temperature and is lower than the melting point. As seen from Fig. 2, the starting point of solidification is about 240 °C where the elastic modulus is increasing. The unknown coefficients ($E_n$, $\delta T_n$, $\tau_n and N$) are found numerically using a non-linear least square fitting with minimum root. By nonlinear regression of data in Fig. 3, the shear elastic modulus $G_{rg}^{'} = E_{rg}/2/(1+\nu_m)$ unknown coefficients are obtained by Eq. (9) and listed in Table 4.

According to the coefficients in Table 4, Eq. (9) does not match the experiments precisely in the melting state for T > 240 °C, where the elastic modulus is in viscous region and shows fluctuations. Estimating the viscous elastic modulus, it results in an average value of $\overline{E_v} = 286 \mp 45(Pa)$. The slight increase of viscous elastic modulus before solidification is interpreted by decreasing of internal energy of the melt and can be proposed as function of temperature in Eq. (10).

$$E_v(T) = -0.52T + 452(Pa) for T > 240^{\circ}C \tag{10}$$

From Eq. (9) and Eq. (10), the viscous-rubbery-glassy expression of elastic modulus can be combined in Eq. (11). According to Eq. (11), during cooling and before the crystallization onset temperature $T > T_c^{onset}$, the thermoplastic is still in the viscous state and solidification does not occur and therefore the denominator of the first term in the right side of Eq. (11) will have a value near one and the elastic modulus simplifies to $E_v$. After the solidification for $T < T_c^{onset}$, the right side of Eq. (11) will converge quickly to the elastic modulus in rubbery glassy $E_{vrg}$, since the denominator of first term tend to be very large and thereby the first term in Eq. (11) becomes zero.

$$E_{vrg} = \frac{E_v - E_{rg}}{1+\exp\left(\frac{T_c^{onset}-T}{ct}\right)} + E_{rg} \tag{11}$$

The constant $ct$ in the Eq. (11) expresses how sharp the transition from viscous to rubbery state goes and must be selected between $10 < ct < 0.01$. In the exponential function the constant $(ct = 0.5)$ enables to model the sudden raise of elastic modulus near solidification point, so that makes the transition possible from low elastic modulus in a viscous state of the thermoplastic to a higher value in rubbery state.

### 4.2. Shrinkage measurements (thermal and crystallization)

Recently, accurate measurements of the thermoset thermal and chemical shrinkage during curing process were carried out and reported for the curing prepregs [19]. For PPS/CF composites and thermoplastic polymer, it is difficult to perform the shrinkage measurements, because of the high processing temperatures; thus, in this research two alternative experimental methods are performed: a novel method using TMA measurement, and an approximate method using the PvT diagram. First

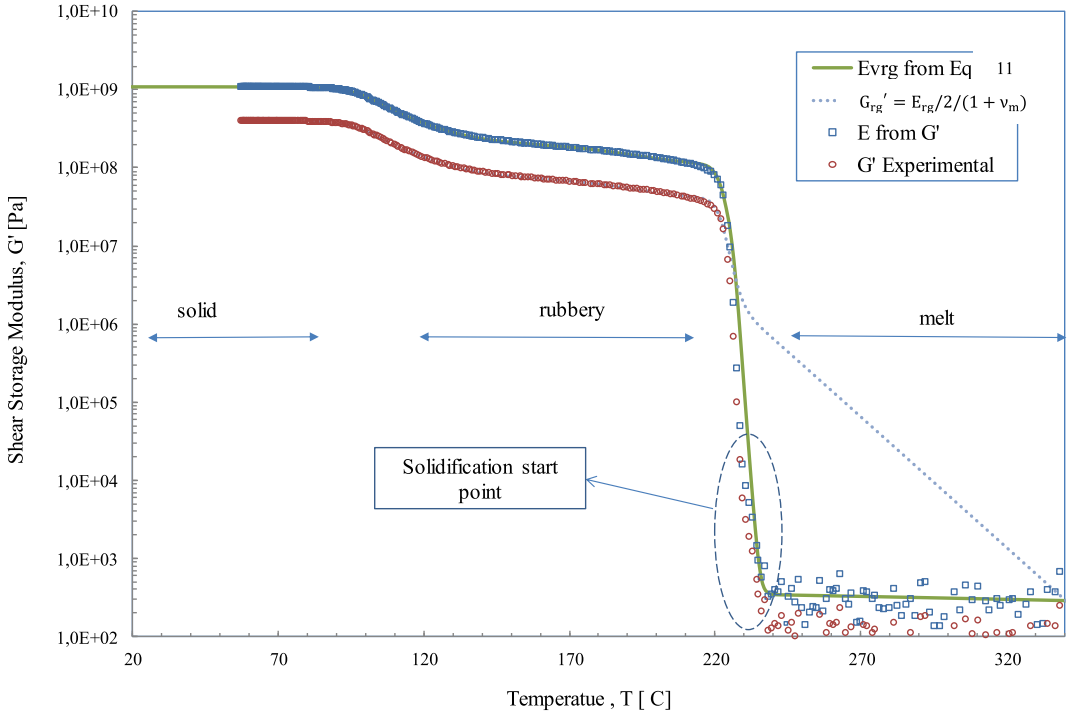


**Fig. 3.** Elastic modulus and the model by cooling of neat thermoplastic PPS.

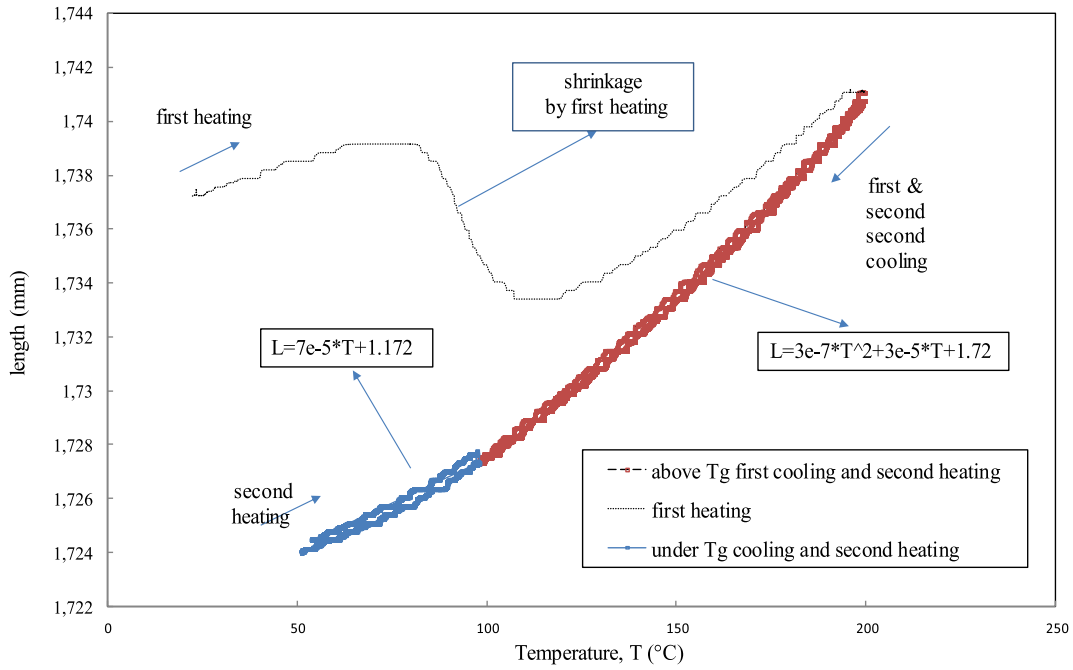


**Fig. 4.** TMA result of transverse extension for consolidate $[0]_{12}$ unidirectional PPS/CF under $T_m$.

of all, the PPS/CF prepregs are consolidated and prepared in different layups to measure the density and to examine the thicknesses uniformity.

### 4.3. TMA measurement for PPS/CF prepreg

As a result, the transverse CTE can be determined and can be seen in Fig. 4. The TMA measurement in Fig. 4, shows a 5 μm ± 2 μm drop after first heating expansion which is observed but no quantity is reported in literature [12]. In the second heating the irreversible contraction (sample length difference of first and second heating) is also observed about 13 μm ± 3 μm while in the literature was 41 μm ± 4 μm after successive heat treatment [12]. As seen in Fig. 4, the PPS/CF expands in the first heating cycle and contracts surprisingly in the glassy transition region; this is also reported, and interpreted as softening and possible cold crystallization, but after the first contraction the sample starts to extend again to 220 °C [12]. However, it seems from the crystallization section presented later (Fig. 7 and Fig. 8), that the reason behind first heating contraction and irreversible contraction are partially related to the cold crystallization, the moisture and the relaxation. In the first cooling the sample contracts as expected, and the slope is higher than during first heating expansion; the contraction by cooling is continued up to $T_g$. The contraction under $T_g$ in the glassy state is nearly linear as the linear fitting shows the least deviation and is repeated by the second heating and cooling, while the nonlinear parabolic regression matches better to expansion and contraction above $T_g$ based on the fitting root mean square less errors. It is obvious that crystallization does not occur in the second cooling and heating cycle; the reason is that the PPS/CF achieves its major crystallization value at the first heating cycle and crystallizes only by cooling and not by a second heating (see Fig. 7 and Fig. 8).

The results in Fig. 5 show that the sample smoothly extends during the first heating below $T_g$, but after that an obvious contraction occurs, which was previously reported only for PPS before by the dilatometer equipment [12]. Thereafter, the sample expands by temperature rise so that the highest expansion at the melt temperature is captured. Increasing the temperature from melt temperature (280 °C for PPS) to process temperature (330 °C) shows a contraction; this contraction could be due to lateral possible squeezing of the sample. When the cooling starts, the molten sample shrinks linearly but at the solidification phase a significant shrinkage decrease happens due to crystallization. By further cooling, the PPS/CF shrinks by a nonlinear manner from the rubbery state to glass temperature, while cooling down below $T_g$ indicates constant shrinkage and linear expansion. The similar linear and quadratic behavior are illustrated in Fig. 4 for below and above $T_g$, respectively.

The maximum PPS/CF shrinkage was measured from the melting $T_m$ to room temperature to be 4.5% and this can be readily found from Fig. 5 (b), while it is not measured easily by the manufacturing process. The total measurable shrinkage is about 3.2% in the thickness direction, which reflects the shrinkage of laminas in the consolidated thermoplastic composite laminate. For the thermoset composite material, characterization of the thermal and chemical shrinkage was carried out during their whole processing cycle thanks to TMA or equivalent methods [31–33]. So, the novelty here is the measuring of the CTE for thermoplastic composite from process to room temperature by TMA as stated in the end of the introduction.

### 4.4. Total shrinkage by PvT diagram

One feasible solution is to extract the Coefficient Volumetric Thermal Expansion (CVTE) for thermoplastics from Pressure specific volume Temperature (PvT) data. For thermoplastic processes like high pressure injection molding, the PvT diagrams are essential and are available for some thermoplastics [34,35]. Fig. 6 shows the PvT diagram for PPS from Toray [36], which was extrapolated here by the authors for thermoplastic at a pressure of 10 bar. The Toray PvT data were given for 20, 40, 80, 100 and 120 MPa and the temperature range of Toray PvT data was 90 °C to 340 °C, so the linear extrapolation was done for 20 bar and 40 bar as shown in Fig. 6. Recently a special new device is developed for high performance thermoplastic to measure the PvT in different pressure and cooling rate [37].

For the semi-crystalline thermoplastic, the shrinkage can be estimated from volume change as in Eq. (12).

$$Totalshrinkage = \frac{1}{V}\frac{dV}{dT} - \gamma_v \frac{dX}{dT} = \beta - \gamma_v \frac{dX}{dT} \tag{12}$$

Where $V$ is the volume replaced in $v$ the specific volume, $T$ is the

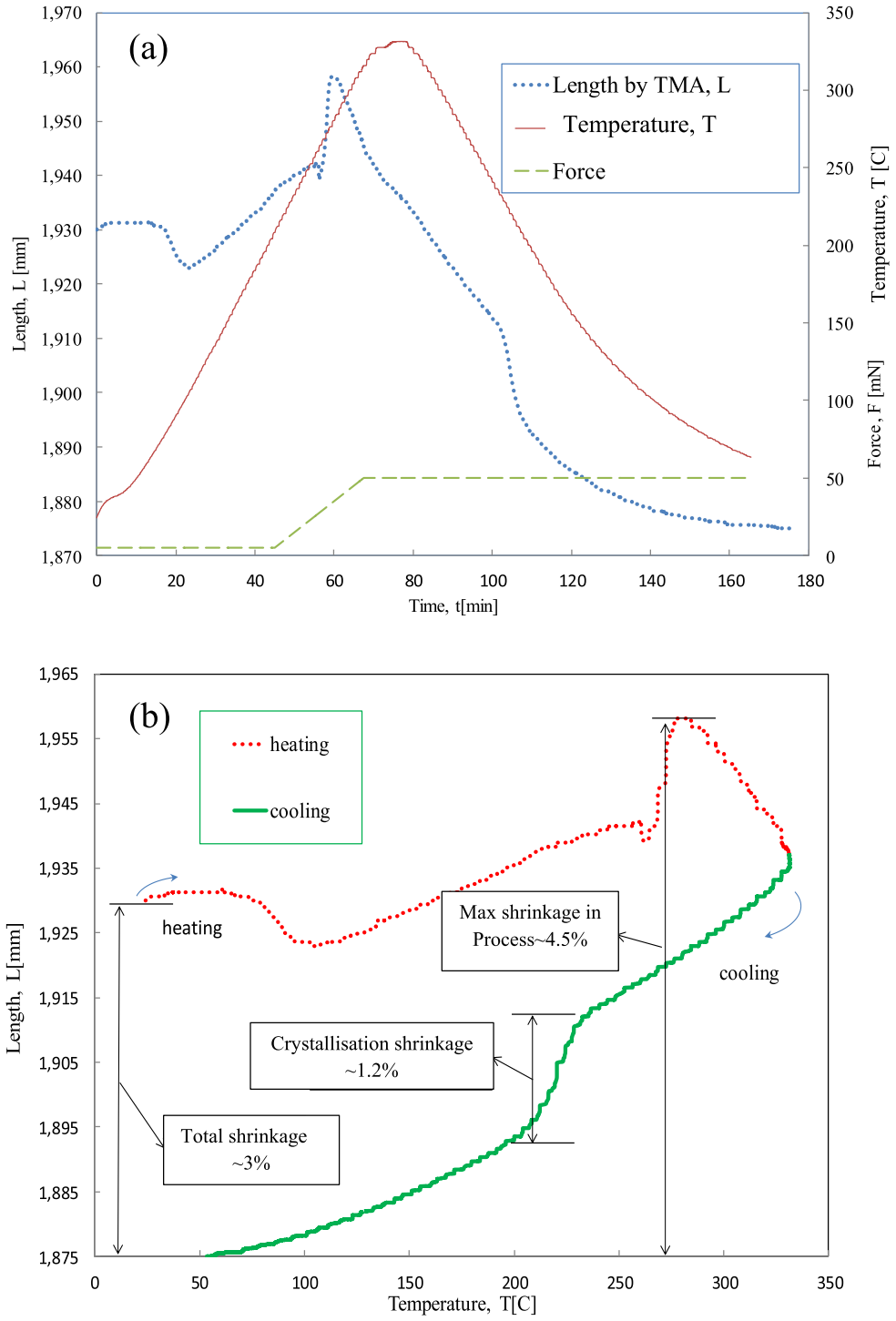


**Fig. 5.** Heating and cooling of PPS/CF consolidated laminate $[0]_{12}$. (a) Length, temperature and force versus time. (b) Length over temperature

temperature, $\gamma_v$ is the volumetric crystallization shrinkage, $X$ is the crystallization rate and $\beta$ is the Coefficient of Volumetric Thermal Expansion or shrinkage ($CVTE$). The shrinkage estimation from volume variations is well known and identical to strain [38], so that the $\alpha = \beta/3$ and the $\gamma = \gamma_v/3$ can be calculated as a function of temperature. For amorphous thermoplastics, the $CVTE$ can be derived from the volume over temperature in Eq. (13). Shrinkage of amorphous thermoplastics without crystallization ($X = 0$) is only thermal shrinkage, named by $\beta$.

$$CVTE = \beta = \frac{1}{V}\frac{dV}{dT} for no crystalinity X = 0 \tag{13}$$

Fig. 6 illustrates the PvT results for PPS [36]. The total shrinkage, estimated CTE, thermal shrinkage and crystallization shrinkage are calculated after applying Eq. (12) to the PvT data.

Another way to extract the CTE from PvT is the direct differentiation of volume with respect to temperature in the mathematical model. An example of a common mathematical model is the PvT Tait model, which is a well fitted model to the PvT diagram. However, the following assumption with negligible error is also reliable: constant shrinkage for glass region ($\alpha_g$) and viscous region ($\alpha_v$) but linear shrinkage in rubbery region ($\alpha_r$). The simplified CTE form can be summarized as in Eq. (14):

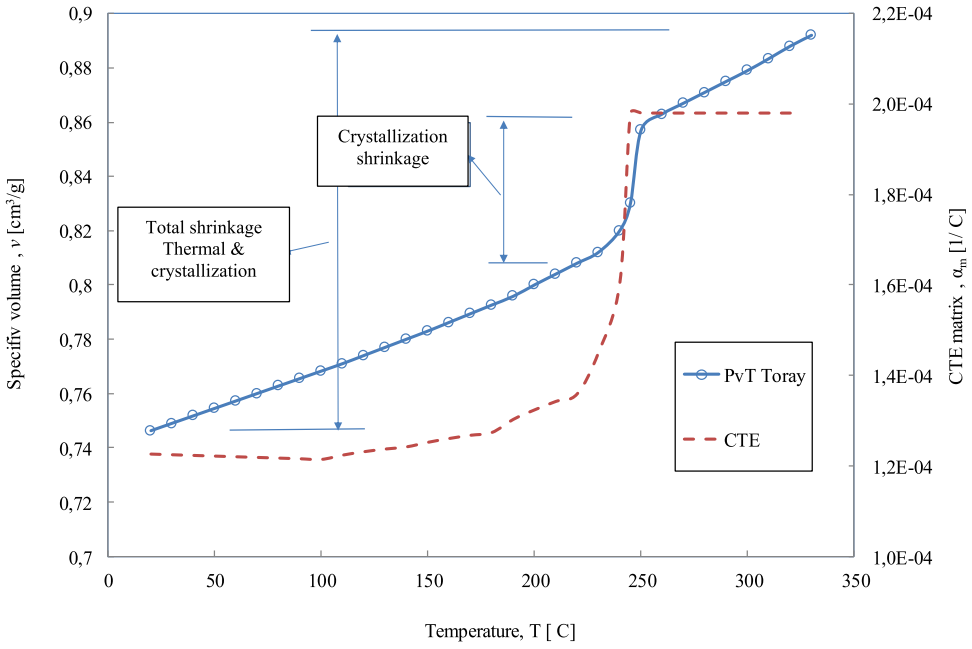


**Fig. 6.** PvT diagram Toray [31] and the extracted total and crystallization shrinkage.

**Table 4**
Coefficients for elastic modulus of neat thermoplastic PPS.

| | n = 1 | n = 2 | n = 3 | n = 4 |
|---|---|---|---|---|
| $E_n$ (MPa) | 173 | 153 | 38.74 | 35.825 |
| $\delta T_n$ (°C) | −102 | −115 | −189 | −222 |
| $\tau_n$ (°C) | 4.932 | 10.74 | 13.03 | 1.635 |

**Table 5**
Degree of crystallization for PPS and PPS/CF.

| Cooling rate (°C/min) | 2 | 5 | 7 | 10 | 20 |
|---|---|---|---|---|---|
| Neat PPS | | | | | |
| ΔH (J/g) | −30.52 | −30.47 | −30.71 | −30.05 | −30.13 |
| X % | 39.9 | 39.8 | 40.1 | 39.3 | 39.4 |
| PPS/CF | | | | | |
| ΔH (J/g) | −9.12 | −9.16 | −8.94 | −8.35 | −6.97 |
| X % | 35.1 | 35.2 | 34.4 | 32.1 | 26.8 |

$$totalshrinkage = \begin{cases} \alpha_g & T^* \le 0 \\ \alpha_r = a.T + b & 0 \le T^* \le T_r \\ \alpha_v & T^* \ge T_r \end{cases} \quad (14)$$

Where $a = \left[(\gamma + \alpha_v) - \alpha_g\right]/T_r$, $b = \left[T_c^{onset}.\alpha_g - T_g.(\gamma + \alpha_v)\right]/T_r$, $T^* = T - T_g$ and $T_r = T_c^{onset} - T_g$ are functions of the crystallization rate. The constant values in Eq. (14) are obtained first by finding the slope of the PvT diagram. The next step is to find $T_g$ and $T_c^{onset}$ from DSC measurement, and to fit the Eq. (12) by constant shrinkage beyond the crystallization part. The fitting is done by least mean square method to $\frac{dV}{dT}$. by assuming constant shrinkage below $T_g$, and above $T_c^{onset}$ and linear shrinkage function for temperatures between glassy and melt states. The result from Eq. (14) and Table 6can be substituted into the micromechanical equations. The viscous state (melt) indicates only thermal shrinkage ($\alpha_v$), but no crystallization shrinkage exists. Just in the rubbery state, the crystallization shrinkage ($\alpha_r$) occurs. Within the solid or glassy (solid) state, the crystallization shrinkage is vanished and thermal shrinkage ($\alpha_g$) arises. The contribution of crystallization shrinkage to total shrinkage is about (1.2/3) = 40% according to Fig. 5, although it depends on the crystallization kinetics.

### 4.5. Crystallization and crystallization kinetics during cooling

When the thermoplastic is cooling down from the process temperature, the crystals can nucleate and grow. Fig. 7 illustrates the heat rate versus temperature for the neat PPS and for as- received PPS/CF prepreg. In the first heating after recording the glass transition temperature to be $T_g \approx 95$℃, the cold crystallization occurred between 125 °C and 145 °C i.e., $T_g < T_c^{cold} < T_m$. The cold crystallization happens to complete the maximum potential crystallization. Later, all crystalline parts melt and the heating continues up to the process temperature and then by cooling down, the crystallizations take place again at 220 °C and 240 °C. By further cooling, the PPS sample shows heat change at the glass transition temperature and finally becomes solid in the glassy state. During cooling, the crystallization occurs above the 125 °C; therefore, as seen in Fig. 7, no crystallization occurs below of 125 °C and only $T_g$ can be detected. The DSC measurements are performed at different cooling rates for a neat PPS/CF and the results are presented in Fig. 8. For the semi-crystalline PPS, different cooling rates are applied in order to investigate the cooling rate effect. The thermoplastic prepreg PPS/CF was tested in the DSC equipment and compared to the neat PPS as in Fig. 8. Five cooling rates were applied on the PPS/CF consecutively, as 20, 10, 7, 5 and 2 (°C/min) in combination with the heating rate of 10 °C/min. The repeated heating by 10 °C/min shows no clear $T_g$ and no cold crystallization, since the maximum crystallization is formed during the first cooling at 10 °C/min. By comparing the five cooling rates, it can be concluded that higher percentage of crystallinity is achieved for higher cooling rate, while this was not reported before. However, by presence of different fiber types, some research has mentioned different crystal growth and DOC in the literature. Lee et al [39] compared the DSC and DMA to determine the crystallinity. In their work, the DSC had higher errors for low crystal content and due to the inherent crystallization.

The DOC of PPS and the PPS/CF prepreg are calculated as a function of fiber weight fraction $X = \frac{\Delta H}{\Delta H^{100\%}\left(1 - W_f\right)}$. The $\Delta H^{100\%}$ is the theoretical enthalpy of fusion for 100% crystalline PPS and is taken here equal to 76.5 J/g [40]. The enthalpy of fusion $\Delta H$ is computed from the area enclosed by the DSC heat flow and the sigmoidal base line in crystallization. The fiber weight fraction is found by $W_f = \frac{\rho_{CF}}{\rho_{PPS}} V_f = \frac{1.8}{1.34} 0.49 = 0.66$ .The DOC for the thermoplastic polymer (PPS) and the PPS/CF

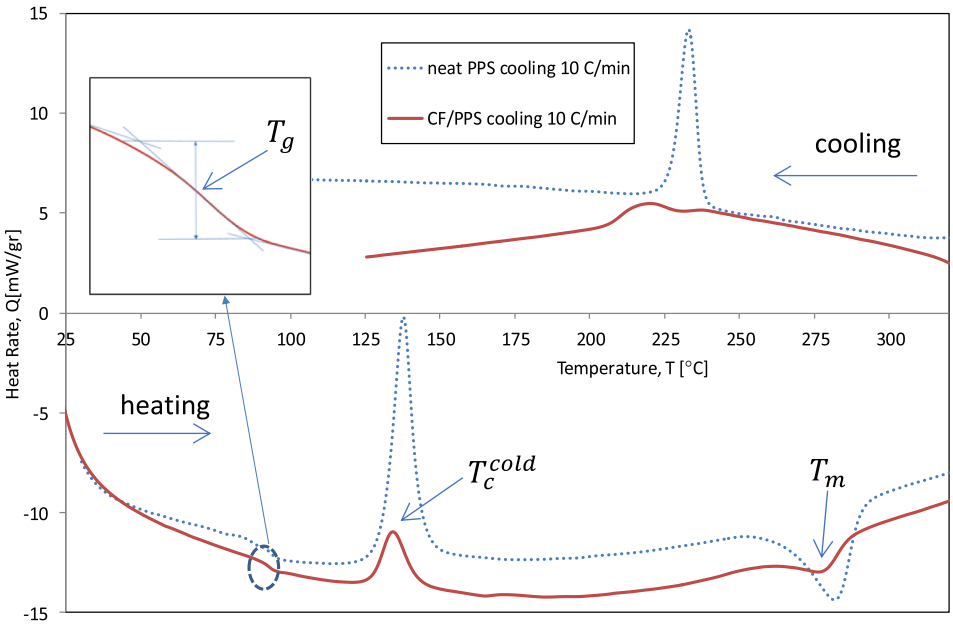


**Fig. 7.** DSC measuring of neat PPS and UD PPS/CF prepregs.

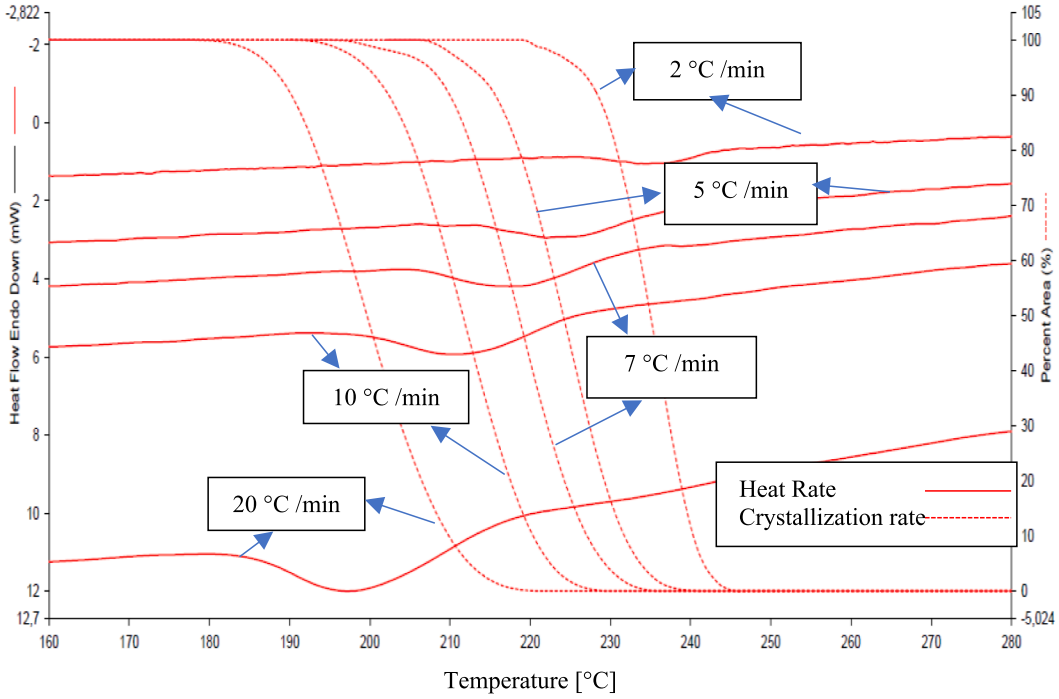


**Fig. 8.** DSC measurements and crystallization rate of PPS/CF with different cooling rates.

prepreg are listed in Table 5 for different cooling rates. Some decrease in the crystallinity was obtained for the higher cooling rates.

Depending on the cooling rate, the crystallizations occur below the melting temperature, and lead to solidification of the semi-crystalline thermoplastic. There are some models available in the literature for time dependent crystallization of PPS and PPS/CF ([39,41]). For a non-isothermal crystallization, the Avrami equation is well known and proved to fit the crystallization kinetics:

$$\psi_c(t) = \frac{X_c(t)}{X_{c\infty}} = 1 - e^{-K(T)t^n} \tag{15}$$

Where $\psi_c(t)$ is the relative crystallinity, $X_c(t)$is the crystallinity, $t$ is time and $X_{c\infty}$ is defined for the maximum crystallinity, $K(T)$ and $n$ are constants from isothermal crystallization. Extending Eq. (15) for non-isothermal crystallization is more applicable for manufacturing induced distortion and residual stress calculations [42,43]. The so-called Nakamura model (Eq. (16)) is proved to have good results [41].

$$\frac{d\psi_c(t)}{dt} = nk(T)(1-\psi_c)(-ln(1-\psi_c))^{\frac{n-1}{n}} \tag{16}$$

Where $k(T) = (K(T))^{1/n} = (ln(2))^{1/n}\left(\frac{1}{t_{1/2}}\right)$ and the $t_{1/2}$ is the half time of

**Table 6**
Shrinkage[1] from different approaches.

| | Method | $\alpha_g$ [2] $T^* \le 0$ | $\alpha_r = a.T+b$ [2] $0 \le T^* \le T_r$ | $\alpha_v$ [2] $T^* \ge T_r$ | $\gamma$ |
|---|---|---|---|---|---|
| PPS | PvT[3] | 120 | 0.7*T + 50 | 190 | 60 |
| PPS/CF | Micromechanics[4] | 71 | 0.36*T + 39 | 110 | 33 |
| (transverse) | TMA[5](220 ↔ 20)°C | 41 | 0.35*T + 17 | NA | NA |
| | TMA[5](330 → 20)°C | 37 | 0.45*T-3.5 | 124 | 38 |

[1] All shrinkage values are in [1e-6/°C] and the uncertainties are about 5%
[2] $\alpha_g$, $\alpha_r and \alpha_v$ are defined in Eq. (14)
[3] fromFig 6
[4] from Eq. (6) and Eq. (7)
[5] Fig. 4 and Fig. 5

crystallization process. In order to find the constants in Eq. (16), a nonlinear curve fitting should be applied to the DSC measurements. The different cooling rates lead to different degrees of crystallinity, as the measurements show several crystallization onset temperatures and kinetics. The melting temperature based on DSC results in heating and cooling, is $T_m = 277 \pm 1$ °C. the onset crystallization is varied according to $T_c^{onset} = 259\left(\frac{dT}{dt}\right)^{-0.023}$ in which $T_c^{onset}$ is the starting crystallization temperature in °C and the $\left(\frac{dT}{dt}\right)$ is the cooling rate in (°C/min). For the crystallization temperature (peak of exothermic crystallization in cooling $T_c^{peak}$) the same relation is valid $T_c^{peak} = 243\left(\frac{dT}{dt}\right)^{-0.021}$.

The relative crystallinity over time is shown in Fig. 9 for 20, 10, 7, 5 and 2 (°C/min) cooling rates. Auer et al. [44] investigated the effect of the melt temperature and time on the crystallinity and have fitted the Avrami model for crystallization kinetics. They investigated different type of fibers and found the Avrami constant to fall in a range from n = 2.1 to 2.7 in PPS composites. However, Leonardo et al. [45] implemented the non-isothermal crystallization to the kinetics using DSC measurements. They determined the Avrami index in the non-isothermal crystallization experiments close to the isothermal one. For dimensional stability, the study on crystallization kinetics and morphology leads to some practical recommendations. For example, Jog et. al. [43] recommended that PPS spends 10–15 s above 190 °C in the mold during cooling and before demolding in order to reach a stable morphology. Kenny and Maffezzoli [41] have investigated the crystallization kinetics of PPS and PPS/CF composites. They determined the Avrami coefficient of the neat PPS to be around 2 and for the PPS/CF composite, the crystallization was less by the same cooling rate, however lower cooling rate may result in more amorphous PPS [41]. Based on these results the non-isothermal measurements will be exploited in future investigations. the crystallization kinetics (Fig. 8 and Fig. 9) can specify the crystallization, its rate and $T_c^{onset}$; thereafter using these quantities, the Eq. (12) and Eq. (13) determine the CTE in glassy, rubbery and melt states as explained before in the PvT section.

### 4.6. Validation of the constitutive model

#### 4.6.1. Validation of total shrinkage for the laminate

For the UD $[0]_{12}$ laminate the total shrinkage values are compared in Table 6 from PvT, micromechanics, TMA and the proposed model. The micromechanics approach, to estimate the CTE in unidirectional composite are close to the experimental results except in the glassy state. The homogenized CTE from micromechanics gives good results in the transverse direction in the rubbery and viscous states. The results from TMA and the micromechanics are listed in Table 6 for comparison. In Table 6 there is a deviation in glassy CTE by micromechanics and TMA, which can be seen by first and second heating in TMA too, this could be due to inexact fiber properties and cold crystallization.

A basic assumption for fibers is to have constant properties with temperatures, while the semi-crystalline thermoplastics have temperature dependent shrinkage. The processing temperatures of thermoplastic composites like PPS/CF reaches a maximum of 400 °C, then the temperature dependent thermoplastic shrinkage is determined by matrix phase change from melt to solid, which depends on contraction and crystallization rates. Therefore, the shrinkage study of PPS/CF needs to consider the cooling rate besides the thermoplastic crystallization

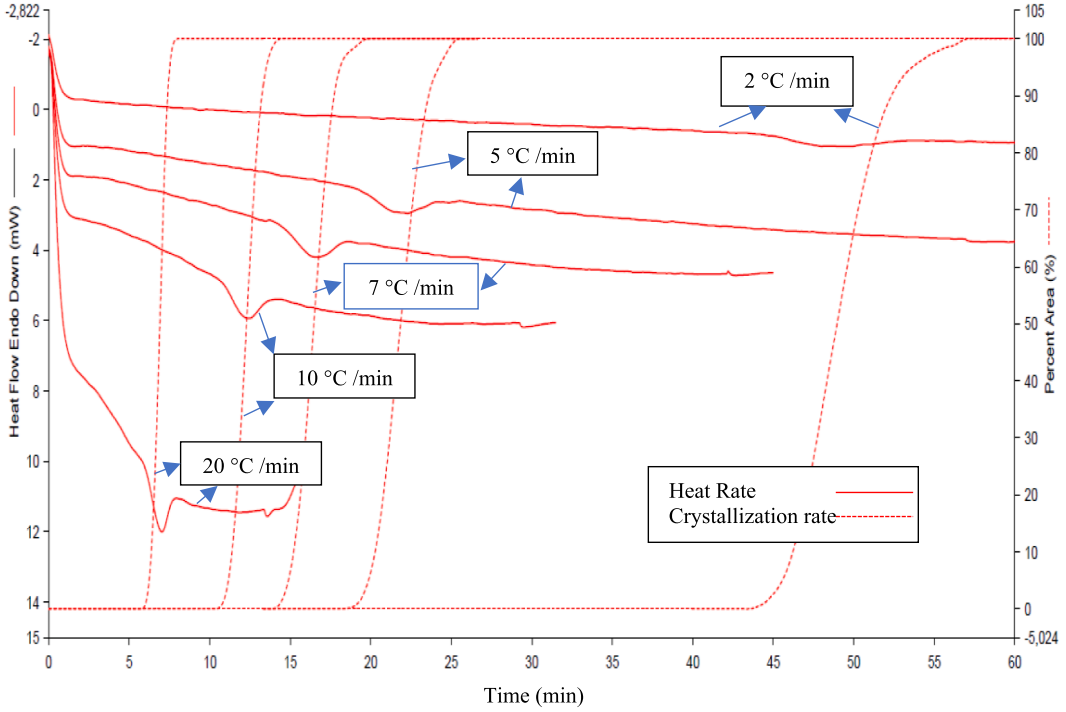


**Fig. 9.** Heat flow and the crystallization rate of PPS/CF prepreg in different cooling down 20, 10, 7, 5 and 2 °C /min respectively.

kinetics.

The values for shrinkage are obtained according to Eq. (14) and are given in Table 6. Fig. 5(b) shows the maximum expansion of prepreg at the melt temperature. For the prepreg, it can be recommended to increase the process pressure before the melting temperature and to hold the pressure after solidification until the glass temperature.

### 4.7. Unsymmetrical laminates

The total experimental shrinkages for unsymmetrical laminates are compared and validated to the model. Using the Classic Lamination Theory (CLT), the deflection of unsymmetrical laminates can be determined. If the curvature is modeled in an incremental form, then Eq. (17) derives the strain and curvature of the laminate:

$$\begin{bmatrix} d\varepsilon \\ d\kappa \end{bmatrix} = \begin{bmatrix} A & B \\ B & D \end{bmatrix}^{-1} \begin{bmatrix} dN^{th} \\ dM^{th} \end{bmatrix} \tag{17}$$

where $d\varepsilon$ and $d\kappa$ are the strain and curvature and A, B and D are the stiffness matrices and $dN^{th}$ is calculated from $dN^{elastic} = dN^{total} - dN^{thermal} - dN^{crystallisation}$. If the material properties change during the cooling and solidification, then Eq. (18) becomes:

$$\begin{bmatrix} \varepsilon \\ \kappa \end{bmatrix} = \int_{T_p}^{T} \begin{bmatrix} A & B \\ B & D \end{bmatrix}^{-1} \begin{bmatrix} dN^{th} \\ dM^{th} \end{bmatrix} dT \tag{18}$$

The closed form of Eq. (18) is derived by Abouhamzeh [4]. The stiffness matrices A, B and D in Eq. (17) and Eq. (18) are calculated using CLT, and the properties are fed into it as a function of temperature, so that the PPS elastic modulus from Eq. (11), the CTE of PPS from Eq. (14) and carbon fiber properties in Table 1, are substituted in the micromechanical formulas [4]. The $dN^{th}$ and $dM^{th}$ are incremental thermal forces and incremental thermal moments respectively, caused by the thermal and crystallization shrinkages.

By DIC method the total part deflection and the curvature are compared in two dimensions in Fig. 10, where the measurements of the deflected parts over their length are illustrated close to the real deflected parts in the same figure. Table 7 indicates the unsymmetrical lay-up curvatures after cooling down from the processing temperature 330 °C to the room temperature 23 °C. The cooling down rate was 10 °C/min. The uncertainty of average curvature measurement from DIC and curvature formula is about 0.09 $(m)^{-1}$. The calculated and measured curvatures show good agreement with a maximum error of 17 %.

## 5. Conclusion

This paper offers a new constitutive model, which is fundamental to estimate and control the thermal shrinkage and crystallization shrinkage of thermoplastic composites. No matter which manufacturing process is taken, e.g., compression molding, autoclave or automated lay-up, the model can be used in process simulation in order to control the composite part dimensions and to avoid unwanted deviations due to warpage. Furthermore, to optimize the process window, the cooling rate dependent solidification and the elastic modulus evolution model can be used.

A high performance prepreg was studied here for thermal shrinkage and crystallization shrinkage of the thermoplastic composite PPS/CF. For this purpose, the total shrinkages from TMA were measured and compared to the PvT diagrams. The proposed method can estimate the shrinkage to reduce and avoid high residual stresses and warpages in complicated parts. Generally, the degree of crystallization and crystallization rate are determined by DSC, and the crystallization rates are measured at different cooling rates. To fit the constitutive model to the

**Table 7**
Curvature of unsymmetrical laminates due to thermal and crystallization shrinkages.

| Lay-up CF/ PPS | Thickness (mm) | $\kappa_{calulated}$ $(m)^{-1}$ | $\kappa_{measured}$ $(m)^{-1}$ | Error % |
|---|---|---|---|---|
| $[0_4/90_4]$ | 1.16 | 3.209 | 3.536 | 10 |
| $[0_3/90/0/90_3]$ | 1.15 | 2.844 | 2.827 | 0.5 |
| $[0_2/90_2]_2$ | 1.14 | 1.082 | 1.269 | 17 |
| $[0/90]_4$ | 1.16 | 0.483 | 0.565 | 17 |

The uncertainty of the laminate thickness values is 0.02 (mm).
The uncertainty of measured curvature values is 0.09 $(m)^{-1}$.

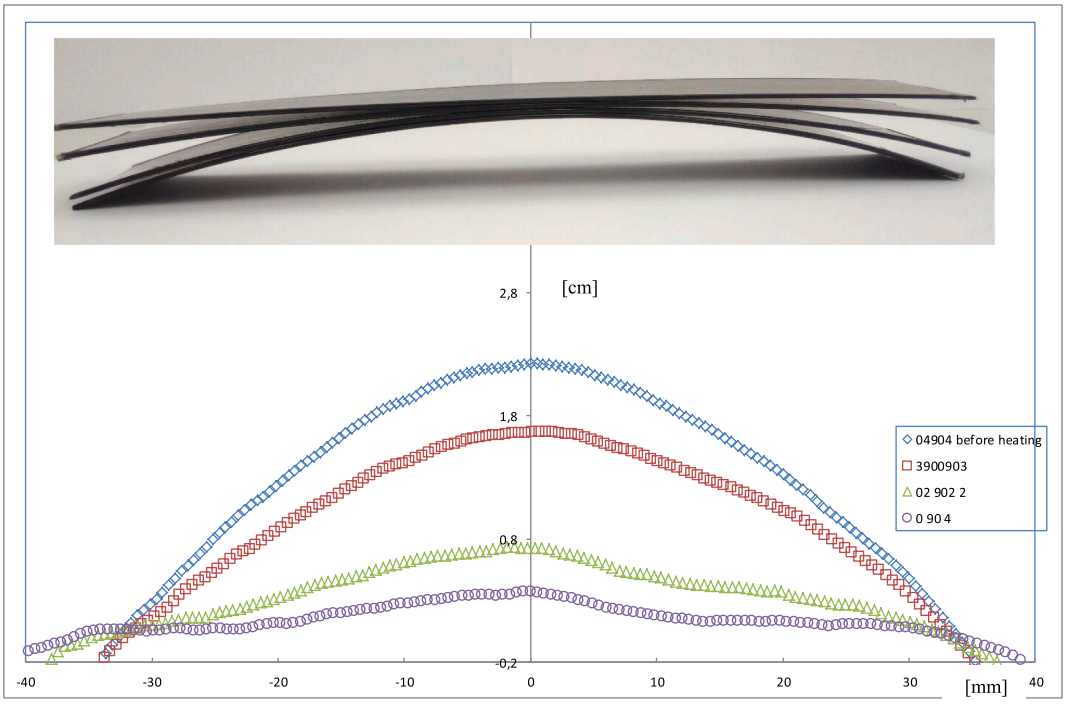


**Fig. 10.** Comparison of deflected part and the DIC measurements.

measured data, a general non-linear least square regression is conducted. To complete the micromechanics, a significant increase of elastic modulus in the onset of crystallization was observed due to viscous to rubbery transformation and successfully modeled. The solidification point was found for the thermoplastic, and thermal dependent solidification model was validated and suggested to apply for all viscous rubbery and glassy moduli in future prediction models.

This work indicates significant results to support the shrinkages for modeling in high performance thermoplastic composites, however, the degree of crystallization in solidification will be exploited using the crystallization kinetics proposed here in future work. Further investigation must be carried out to complete the engineering basis for more precise composite parts assembly. It is indeed interesting to develop the effect of other laminate lay-up and to study the quasi-isotropic laminates for multidirectional loading in aerospace structures. Additional studies can extend the dimensional stability and tolerances in thermoplastic composite during automated manufacturing.

### *CRediT authorship contribution statement*

**M. Golzar:** Conceptualization, Methodology, Software, Validation, Writing – original draft. **J. Sinke:** Resources, Writing – review & editing. **M. Abouhamzeh:** Visualization, Writing – review & editing.

### Declaration of Competing Interest

The authors declare that they have no known competing financial interests or personal relationships that could have appeared to influence the work reported in this paper.

### Acknowledgment

M. Golzar would like to thank Tarbiat Modares University research affair for the granting the sabbatical stay (Grant IDs 11/3221,1396/02/14) at the Delft University of Technology (TUD). Also, the Faculty of Aerospace Engineering at the Technical University of Delft is appreciated for the cooperation and for the lab facilities.

### References

[1] Parlevliet PP, Bersee HEN, Beukers A. Residual stresses in thermoplastic compositesA study of the literature-Part I: Formation of residual stress. Compos Part A Appl Sci Manuf 2007;38(3):651–65.
[2] Parlevliet PP, Bersee HEN, Beukers A. Residual stresses in thermoplastic composites-A study of the literature-Part II: Experimental techniques. Compos Part A Appl Sci Manuf 2007;38(3):651–65.
[3] Abouhamzeh M, Sinke J, Jansen KMB, Benedictus R. Kinetic and thermo-viscoelastic characterisation of the epoxy adhesive in GLARE. Compos Struct 2015;124:19–28.
[4] Abouhamzeh M, Sinke J, Jansen KMB, Benedictus R. Closed form expression for residual stresses and warpage during cure of composite laminates. Compos Struct 2015;133:902–10.
[5] Abouhamzeh M, Sinke J, Benedictus R. Investigation of curing effects on distortion of fibre metal laminates. Compos Struct 2015;122:546–52.
[6] Chapman TJ, Gillespie JW, Pipes RB, Manson J-A-E, Seferis JC. Prediction of Process-Induced Residual Stresses in Thermoplastic Composites. J Compos Mater 1990;24(6):616–43.
[7] Lawrence WE, Seferis JC. Mater Response 1992;13(2):86–96.
[8] Barnes JA, Simms IJ, Farrow GJ, Jackson D, Wostenholm G, Yates B. Expansion Behaviour of Thermoplastic Composite Materials. J Thermoplast Compos Mater 1990;3(January):66–80.
[9] Trende A, Astroem BT, Nilsson G. Modelling of residual stresses in compression moulded glass-mat reinforced thermoplastics. Compos Part A Appl Sci Manuf 2000;31(11):1241–54.
[10] Kim B, Bernet N, Sunderland P, Manson JA. Numerical Analysis of the dimensional stability of thermoplastic composite using a thermoviscoelastic approach. J Compos Mater 2002;36(20):2389–403.
[11] Brauner C, Peters C, Brandwein F, Herrmann AS. Analysis of process-induced deformations in thermoplastic composite materials. J Compos Mater 2014;48(22):2779–91.
[12] Greisel M, Jäger J, Moosburger-Will J, Sause MGR, Mueller WM, Horn S. Influence of residual thermal stress in carbon fiber-reinforced thermoplastic composites on interfacial fracture toughness evaluated by cyclic single-fiber push-out tests. Compos Part A Appl Sci Manuf 2014;66:117–27.
[13] Batista NL, Rezende MC, Botelho EC. Effect of crystallinity on CF/PPS performance under weather exposure: moisture, salt fog and UV radiation. Polym Degrad Stab 2018;153:255–61.
[14] Liu Y, Zhou X, Wang Z. Effect of isothermal heat treatment on crystallinity, tensile strength and failure mode of CF/PPS laminate. High Perform Polym 2021. https://doi.org/10.1177/0954008320969843.
[15] Lee WI, Springer GS. A Model of the Manufacturing Process of Thermoplastic Matrix Composites. J Compos Mater 1987;21(11):1017–55.
[16] Sim WM. Challenges of residual stress and part distortion in the civil airframe industry. Int J Microstruct Mater Prop 2010;5(4/5):446. https://doi.org/10.1504/IJMMP.2010.037621.
[17] Wijskamp S. Shape distortions in composites forming. The Netherlands: University of Twente, Enschede; 2005. Ph.D. thesis.
[18] Baran I, Akkerman R, Hattel JH. Material characterization of a polyester resin system for the pultrusion process. Compos Part B Eng 2014;64:194–201.
[19] Kravchenko OG, Kravchenko SG, Pipes RB. Chemical and thermal shrinkage in thermosetting prepreg. Compos Part A Appl Sci Manuf 2016;80:72–81.
[20] DSML, https://www.tudelft.nl/en/ae/organisation/departments/dasml", 2021.
[21] Kapton and P. Film, "https://www.dupont.com/electronic-materials/kapton-polyimide-film.html", 2021.
[22] Péron M, Jacquemin F, Casari P, Orange G, Bikard J, Bailleul J-L, et al. Measurement and prediction of residual strains and stresses during the cooling of a glass fibre reinforced PA66 matrix composite. Compos A Appl Sci Manuf 2020;137.
[23] Material Physical Labrotary, "https://www.tudelft.nl/lr/organisatie/afdelingen/aerospace-structures-and-materials/novel-aerospace-materials/facilities/material-physics-lab/.", 2021.
[24] Ding A, Li S, Wang J, Zu L. A three-dimensional thermo-viscoelastic analysis of process-induced residual stress in composite laminates. Compos Struct 2015;129:60–9.
[25] Ding A, Li S, Sun J, Wang J, Zu L. A comparison of process-induced residual stresses and distortions in composite structures with different constitutive laws. J Reinf Plast Compos 2016;35(10):807–23.
[26] Jeronimidis G, Parkyn aT. Residual Stresses in Carbon Fibre-Thermoplastic Matrix Laminates. J Compos Mater 1988;22(5):401–15.
[27] Péron M, Jacquemin F, Casari P, Orange G, Bailleul JL, Boyard N. Thermo-mechanical characterization of a thermoplastic composite and prediction of the residual stresses and lamina curvature during cooling. AIP Conf Proc 2017;1896.
[28] Abouhamzeh M, Sinke J, Jansen KMB, Benedictus R. A new procedure for thermo-viscoelastic modelling of composites with general orthotropy and geometry. Compos Struct 2015;133:871–7.
[29] R.A. Schapery, Thermal Expansion Coefficent of Composite Materials Based on Energy Principles, 2(3) (1968) 380–404.
[30] Golzar M. Melt spinning of fine PEEK filaments. PhD thesis, TU Dresden 2004.
[31] Moretti L, Castanié B, Bernhart G, Olivier P. Characterization and modelling of cure-dependent properties and strains during composites manufacturing. J Compos Mater 2020;54:3109–24.
[32] Péron M, Cardinaud R, Lefèvre N, Aubril J, Sobotka V, Boyard N, et al. PvT-HADDOC: A multi-axial strain analyser and cure monitoring device for thermoset composites characterization during manufacturing. Compos A 2017;101:129–42.
[33] Sfar Zbed R, Le Corre S, Sobotka V. Process-induced strains measurements through a multi-axial characterization during the entire curing cycle of an interlayer toughened Carbon/Epoxy prepreg. Compos A Appl Sci Manuf 2022;153:106689.
[34] Wang J. PVT Properties of Polymers for Injection Molding. Some Crit. Issues Inject: Molding, InTech Publisher; 2012.
[35] Zoller P, Walsh DJ. Standard Pressure-Volume-Temperature data for polymers. Lancaster: Technomic Publishing Co., Inc.; 1995.
[36] Toray, "https://www.toray.jp/plastics/en/torelina/technical/index.html ", 2021.
[37] Pignon B, Tardif X, Lefèvre N, Sobotka V, Boyard N, Delaunay D. A new PvT device for high performance thermoplastics: Heat transfer analysis and crystallization kinetics identification. Polym Test 2015;45:152–60.
[38] Zarrelli M, Skordos AA, Partridge IK. Investigation of cure induced shrinkage in unreinforced epoxy resin. Plast Rubber Compos 2002;31(9):377–84.
[39] Lee TH, Boey FYC, Khor KA. On the determination of polymer crystallinity for a thermoplastic PPS composite by thermal analysis. Compos Sci Technol 1995;53(3):259–74.
[40] Motta Dias MH, Jansen KMB, Luinge JW, Bersee HEN, Benedictus R. Effect of fiber-matrix adhesion on the creep behavior of CF/PPS composites: temperature and physical aging characterization. Mech Time Depend Mater 2016;20(2):245–62.
[41] Kenny JM, Maffezzoli A. Crystallization kinetics of poly(phenylene sulfide) (PPS) and PPS/carbon fiber composites. Polym Eng Sci 1991;31(8):607–14.
[42] Mubarak Y, Harkin-Jones EMA, Martin PJ, Ahmad M. Modeling of non-isothermal crystallization kinetics of isotactic polypropylene. Polymer (Guildf) 2001;42(7):3171–82.
[43] Jog JP, Nadkarni VM, Science P. Crystallization Kinetics of Polyphenylene Sulfide *. J Appl Polym Sci 1985;30(3402):997–1009.
[44] Auer C, Kalinka G, Krause Th, Hinrichsen G. Crystallization Kinetics of Pure and Fiber-Reinforced Poly (phenylene Sulfide). J Appl Polym Sci 1994;51(3):407–13.
[45] López LC, Wilkes GL. Non-isothermal crystallization kinetics of poly(p-phenylene sulphide). Polymer 1989;30(5):882–7.